Electron degradation and thermalization in H_2 gas

Ken-ichi Kowari*
Atomic Physics Laboratory, The Institute of Physical and Chemical Research (RIKEN), 2-1 Hirosawa, Wako-shi, Saitama 351-01, Japan
(Received 17 April 1995; revised manuscript received 22 August 1995)

Thermalization and degradation of subexcitation electrons with initial energies of 1, 3, and 5 eV in H_2 gas at a number density of 2.69×10^{19} cm^{-3} and a temperature of 300 K are studied through a numerical solution of the Boltzmann equation. The collision term in the Boltzmann equation includes contributions from elastic collisions as well as inelastic collisions, viz., collisions leading to rotational and vibrational excitation or deexcitation. The time evolution of the electron energy distribution function and of the cumulative degradation spectrum, as well as thermalization times, are calculated. Time-dependent yields or collision numbers for rotationally and vibrationally inelastic processes are calculated by using the cumulative degradation spectrum. We discuss extensively the present result for thermalization times in comparison with experimental data and other theoretical results.

PACS number(s): 34.10.+x, 34.50.Bw, 31.70.Hq, 34.50.Ez

I. INTRODUCTION

Electrons with energies below the lowest electronic threshold energy of the major constituent molecule of a gas, of which molecules are present in a large excess compared to the total number of the electrons, relax due to elastic collisions, vibrationally inelastic collisions, rotationally inelastic collisions, and chemically reactive processes such as electron attachment. These electrons were termed subexcitation electrons by Platzman [1].

In previous papers [2,3], time-dependent studies on the degradation and thermalization of the subexcitation electrons in CH_4 [2] and SiH_4 [3] were carried out with the method developed by Kowari *et al.* [2]. The method is based on the Boltzmann equation with the Fokker-Planck operator for elastic collisions and a difference operator for inelastic collisions. Although the difference operator involving rotationally inelastic collisions as well as vibrationally inelastic collisions has been presented formally, the rotationally inelastic collisions were not included explicitly in the previous calculations because the momentum transfer cross sections employed for CH_4 and SiH_4 were vibrationally elastic. The present choice of H_2 gives us an advantage in including the rotationally inelastic collisions explicitly in calculations: we do not need to consider many rotational states at room temperature because the rotational threshold energy of H_2 is large.

A theoretical approach for the study of electrons due to elastic collisions in the low energy regime near thermal equilibrium based on the Fokker-Planck equation was considered by Shizgal and co-workers [4–6]. A review of work was presented by Shizgal *et al.* [7]. The approach is referred to as the quadrature discretizing method (QDM). Another method, proposed by Shizgal and Nishigori [8], transforms the Fokker-Planck equation to a Schrödinger equation, and applies a WKB method of solution. This approach was further developed in Refs. [9–11].

In radiation physics and chemistry, the Spencer-Fano equation [12] has been widely used to study the degradation of electrons in various gases [13–16]. Because the energy region of primary interest is much higher than the thermal energy, the temperature of a gas is disregarded. This is referred to as the cold gas approximation (CGA). Naturally, the Spencer-Fano equation is not applicable to the energy region near the thermal energy. As is shown in the previous papers [2,3], the Boltzmann equation with the CGA is equivalent to the Spencer-Fano equation. The crucial difference between the Boltzmann equation and the Spencer-Fano equation is whether the temperature of the gas is taken into account. Studies with the Spencer-Fano analysis were reviewed in Refs. [17,18].

To put the present work in perspective, it is appropriate to summarize some experimental and theoretical studies on the degradation and thermalization of subexcitation electrons in H_2 gas. One key quantity is the electron thermalization time. The thermalization time literally means a time until electrons thermalize; however, in practice the term ''thermalization time'' is used in different contexts. Assuming that the average energy of electrons decreased exponentially with time, Warman and Sauer [19] measured the thermalization time $\tau_{1.1}$ in H_2. The thermalization time $\tau_{1.1}$ is a time until the average energy of electrons reaches 10% above the thermal energy. Hatano and his co-workers [20,21] found that the average energy of electrons in the energy region close to the thermal energy decreases exponentially with time by using the microwave-power-absorption method they developed [20], and they have reported the decay constant of the exponential function for H_2 as the thermalization time [21]. Koura [22,23] carried out a study on H_2 by using Monte Carlo simulations and determined the thermalization time $\tau_{1.1}$. Kimura, Krajar-Bronić, and Inokuti [16] studied the degradation of the subexcitation electrons in H_2 by using the Spencer-Fano equation with and without the continuous slowing-down approximation (CSDA). Kimura *et al.* [16] obtained the thermalization time consistent with other studies [24,25] using the CSDA. Yields of vibrationally inelastic and

*Present address: c/o Dr. M. Matsuzawa, Department of Applied Physics and Chemistry, The University of Electro-Communications, 1-5-1 Chofu-ga-oka, Chofu-shi, Tokyo 182, Japan.

rotationally inelastic processes are important in astrophysics as well as radiation physics and chemistry. Douthat [26] showed that subexcitation electrons are crucial to the vibrational and rotational yields of H_2 in interstellar clouds. The yields of vibrational and rotational processes of H_2 were also given by Kimura *et al.* [16]. The isotope effects were studied theoretically in Refs. [16,23], and experimentally in Ref. [21].

II. THE BOLTZMANN EQUATION

The theoretical method used here is the same as in Refs. [2,3], and has been described in detail in Ref. [2]. We provide a brief description of the theory for completeness. We consider a system consisting of a relatively small number of subexcitation electrons dispersed throughout a molecular gas. We assume that the electron distribution function is spatially homogeneous because no electric field is applied to the system.

We use the Boltzmann equation, which explicitly includes elastic and inelastic collisions, as given by

$$\frac{\partial f}{\partial t}=J_{\rm el}(f)+J_{\rm in}(f), \tag{1}$$

where $f=f(\mathbf{v},t)$. In Eq. (1), $J_{\rm el}(f)$ and $J_{\rm in}(f)$ are the elastic and inelastic collision operators, respectively. We denote the mass of an electron by m and that of a molecule by M. Applying the expansion in terms of the small mass ratio m/M in the elastic term, we obtain the differential Fokker-Planck operator

$$J_{\rm el}=\frac{mN_b}{Mv^2}\frac{\partial}{\partial v}\left[v^4\sigma_m(v)\left(1+\frac{kT}{mv}\frac{\partial}{\partial v}\right)\right]f(v), \tag{2}$$

where N_b is the number density of moderator molecules, k the Boltzmann constant, T the temperature of the moderator, v the speed of an electron, and $\sigma_m(v)$ the momentum transfer cross section.

The inelastic collision operator can be written as the sum over all the inelastic processes involved and can be cast in the form of a difference operator. The derivation of the inelastic collision operator is given in the Appendix of Ref. [2]. Suppose that $\sigma_{ij}(v)$ is the cross section for an inelastic process in which a molecule makes a transition from state i to state j. Then the inelastic collision operator is given as

$$J_{\rm in}=N_b v\sum_{i,j}\left(n_i\frac{v'^2}{v^2}\sigma_{ij}(v')f(v')-n_i\sigma_{ij}(v)f(v)\right), \tag{3}$$

where $v'=\sqrt{v^2-(2\epsilon_{ij}/m)}$, and $\epsilon_{ij}=\epsilon_j-\epsilon_i$ is the energy transfer for internal molecular states i and j. The population density of the molecular state is denoted by n_i, and $\Sigma_i n_i=1$.

The Boltzmann equation becomes

$$\frac{\partial f}{\partial t}=\frac{mN_b}{Mv^2}\frac{\partial}{\partial v}\left[v^4\sigma_m(v)\left(1+\frac{kT}{mv}\frac{\partial}{\partial v}\right)\right]f(v)+N_b v\sum_{i,j}\left(n_i\frac{v'^2}{v^2}\sigma_{ij}(v')f(v')-n_i\sigma_{ij}(v)f(v)\right). \tag{4}$$

In radiation physics and chemistry, it is customary to use the density per unit energy range,

$$\rho(E,t)\equiv 2\pi\left(\frac{2}{m}\right)^{3/2}\sqrt{E}f(v,t), \tag{5}$$

where $E=mv^2/2$, and also the track-length distribution (or incremental degradation spectrum)

$$z(E,t)\equiv v\rho(E,t). \tag{6}$$

Inserting Eqs. (5) and (6) in Eq. (4), we obtain the equation for time evolution of *z(E,t)*; viz.,

$$\frac{1}{v}\frac{\partial z(E,t)}{\partial t}=\frac{2N_b m}{M}\frac{\partial}{\partial E}\left\{E\sigma_m(E)z(E,t)+E^2\sigma_m(E)kT\frac{\partial}{\partial E}\left[\frac{z(E,t)}{E}\right]\right\}+N_b\sum_{i,j}\left[n_i\sigma_{ij}(E')z(E',t)-n_i\sigma_{ij}(E)z(E,t)\right], \tag{7}$$

where $E'\equiv\frac{1}{2}mv'^2=E+\epsilon_{ij}$. The process ij is inelastic if $i<j$, and ϵ_{ij} is positive. On the other hand, the process ij is superelastic if $i>j$, and ϵ_{ij} is negative.

We consider the relaxation of electrons in a gas due to elastic and inelastic collisions. Inelastic collisions that may be important in the low energy regime are rotational and vibrational collisions. The cross section for rotational excitation from a rotational state J to J' is denoted by $\sigma_{rot}^{JJ'}$ and the energy transfer by $E^{JJ'}$. The cross section for vibrational excitation from a vibrational state V to V' in the vibrational mode ν is denoted by $\sigma_\nu^{VV'}$ and the energy transfer by $E_\nu^{VV'}$. The population density of the vibrational state V in the vibrational mode ν is denoted by n_ν^V. It is necessary to replace the summation $\Sigma_{i,j}\equiv\Sigma_i\Sigma_j$ with an explicit reference to the rotational and vibrational states, viz.,

$$\sum_i\sum_j=\sum_J\sum_{J'}+\sum_\nu\sum_V\sum_{V'}. \tag{8}$$

The Boltzmann equation with the differential operator for elastic collisions and the difference operator for inelastic collisions is

$$\frac{1}{v}\frac{\partial z(E,t)}{\partial t}=\frac{2N_b m}{M}\left\{\left[\frac{\partial}{\partial E}E\sigma_m(E)z+\frac{\partial}{\partial E}[E^2\sigma_m(E)]kT\frac{\partial}{\partial E}\left(\frac{z}{E}\right)+E^2\sigma_m(E)kT\frac{\partial^2}{\partial E^2}\left(\frac{z}{E}\right)\right]\right\}+N_b\left[\sum_J n_{\rm rot}^J\sum_{J'}\sigma_{\rm rot}^{JJ'}(E+E^{JJ'})z(E+E^{JJ'},t)+\sum_\nu\sum_V n_\nu^V\sum_{V'}\sigma_\nu^{VV'}(E+E_\nu^{VV'})z(E+E_\nu^{VV'},t)-\sum_J n_{\rm rot}^J\sum_{J'}\sigma_{\rm rot}^{JJ'}(E)z(E,t)-\sum_\nu\sum_V n_\nu^V\sum_{V'}\sigma_\nu^{VV'}(E)z(E,t)\right]+\delta(E-E_0)\delta(t). \quad (9)$$

In Eq. (9), the last term on the right-hand side shows the source of electrons at a fixed energy E_0 and at a fixed time $t=0$.

The cumulative degradation spectrum defined as

$$Z(E,t)=\int_0^t z(E,t)dt \quad (10)$$

is an important notion in radiation physics and chemistry. From Eqs. (9) and (10) we obtain

$$\frac{1}{v}\frac{\partial Z(E,t)}{\partial t}=\frac{2N_b m}{M}\left\{\left[\frac{\partial}{\partial E}E\sigma_m(E)Z+\frac{\partial}{\partial E}[E^2\sigma_m(E)]kT\frac{\partial}{\partial E}\left(\frac{Z}{E}\right)+E^2\sigma_m(E)kT\frac{\partial^2}{\partial E^2}\left(\frac{Z}{E}\right)\right]\right\}+N_b\left[\sum_J n_{\rm rot}^J\sum_{J'}\sigma_{\rm rot}^{JJ'}(E+E^{JJ'})Z(E+E^{JJ'},t)+\sum_\nu\sum_V n_\nu^V\sum_{V'}\sigma_\nu^{VV'}(E+E_\nu^{VV'})Z(E+E_\nu^{VV'},t)-\sum_J n_{\rm rot}^J\sum_{J'}\sigma_{\rm rot}^{JJ'}(E)Z(E,t)-\sum_\nu\sum_V n_\nu^V\sum_{V'}\sigma_\nu^{VV'}(E)Z(E,t)\right]+\delta(E-E_0). \quad (11)$$

Once the cumulative degradation spectrum is obtained, the time-dependent yield or collision number $n_{lm}(t)$ for a collision process *lm* is calculated straightforwardly as

$$n_{lm}(t)=N_b n_l\int_{E_{lm}}^\infty Z(E,t)\sigma_{lm}(E)dE, \quad (12)$$

where E_{lm} is the threshold energy of the process *lm*.

With the CGA, Eq. (9) can be written as

$$\frac{1}{v}\frac{\partial z(E,t)}{\partial t}=\frac{2N_b m}{M}\frac{\partial}{\partial E}[E\sigma_m(E)z(E,t)]+N_b\left[\sum_{J'}\sigma_{\rm rot}^{0J'}(E+E^{0J'})z(E+E^{0J'},t)+\sum_\nu\sum_{V'}\sigma_\nu^{0V'}(E+E_\nu^{0V'})z(E+E_\nu^{0V'},t)\right]-N_b\left[\sum_{J'}\sigma_{\rm rot}^{0J'}(E)z(E,t)-\sum_\nu\sum_{V'}\sigma_\nu^{0V'}(E)z(E,t)\right]+\delta(E-E_0)\delta(t). \quad (13)$$

Applying the CSDA to Eq. (13), i.e., expanding the equation up to linear terms in the excitation energy for each process corresponding to rotationally and vibrationally inelastic collision terms, we obtain

$$\frac{1}{v}\frac{\partial z(E,t)}{\partial t}=N_b\frac{\partial}{\partial E}[s(E)z(E,t)], \quad (14)$$

where *s(E)* is the stopping cross section given by

$$s(E)=\frac{2m}{M}E\sigma_m(E)+\sum_J E^{0J}\sigma_{\rm rot}^{0J}+\sum_\nu\sum_V E_\nu^{0V}\sigma_\nu^{0V}. \quad (15)$$

The CSDA time, defined by

$$\tau(E)=\int_E^{E_0}\frac{dE}{N_b v s(E)}, \quad (16)$$

means an approximate time in which the average energy of electrons relaxes from E_0 to E. From the solution of Eq. (9), we can obtain the average energy of electrons without approximation. The average energy of the electrons at time *t* using the electron density distribution function at that time is given by

$$E_{\rm avg}=\frac{\int_0^\infty E\rho(E,t)dE}{\int_0^\infty\rho(E,t)dE}. \quad (17)$$

III. INPUT CROSS-SECTION DATA

A cross-section set for H_2 used for the present calculation consists of the momentum transfer cross section, rotationally inelastic cross sections, and vibrationally inelastic cross sections. The vibrationally inelastic cross sections used here are

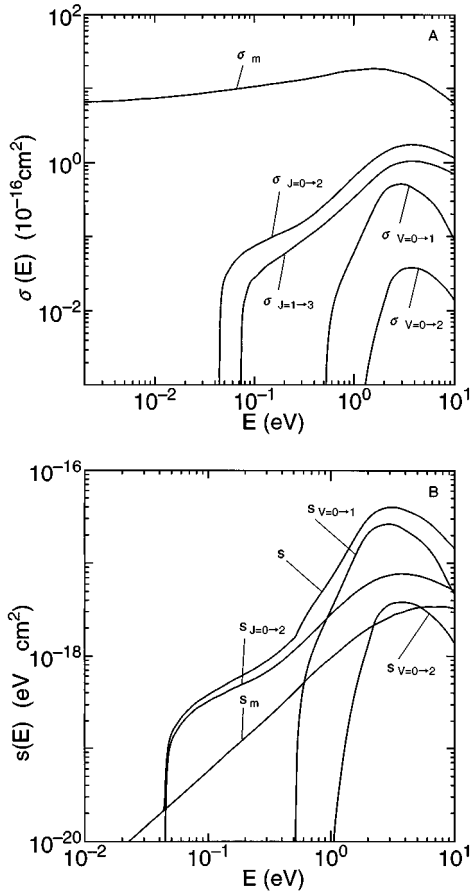

FIG. 1. (A) A set of momentum transfer cross section σ_m, vibrational cross sections $\sigma_{V=0\to1}$ for $V=0$ to 1 and $\sigma_{V=0\to2}$ for $V=0$ to 2, and rotational cross sections $\sigma_{J=0\to2}$ for $J=0$ to 2 and $\sigma_{J=1\to3}$ for $J=1$ to 3 is shown. The momentum transfer cross section and vibrational cross sections are those of Buckman and Phelps. The rotational cross sections are those of England *et al.* (B) The stopping cross section s_m for the momentum transfer process, stopping cross section $s_{V=0\to1}$ for $V=0$ to 1, stopping cross section $s_{V=0\to2}$ for $V=0$ to 2, stopping cross section $s_{J=0\to2}$ for $J=0$ to 2, and stopping cross section s are shown. The stopping cross section s is the sum of s_m, $s_{V=0\to1}$, $s_{V=0\to2}$, and $s_{J=0\to2}$.

those unresolved in purely vibrational excitation and simultaneous vibrational-rotational excitation. In other words, the present vibrational inelastic cross sections include cross sections for simultaneous vibrational-rotational excitation as well as purely vibrational excitation. Figure 1(A) shows the momentum transfer cross section, vibrationally inelastic cross sections for $V=0$ to 1 and $V=0$ to 2, and the rotationally inelastic cross sections $J=0$ to 2 and $J=1$ to 3. The momentum transfer cross section and vibrationally inelastic cross sections are those adopted by Buckman and Phelps [27]. The vibrationally inelastic cross sections we need here are those for $V=0$ to 1 and $V=0$ to 2. The vibrational threshold energies for $V=0$ to 1 and $V=0$ to 2 are 0.516 and 1.00 eV, respectively.

We need also the rotationally inelastic cross sections for the transitions with J to $J+2$ where J is up to 6. The rotationally inelastic cross sections for $J=0$ to 2, 1 to 3, 2 to 4, and 3 to 5 are taken from the data of England *et al.* [28]. The rest of the rotationally inelastic cross sections, that is, those for $J=4$ to 6, 5 to 7, and 6 to 8 are obtained from the scaling law

$$\sigma(J\to J+2)=\frac{3(J+1)(J+2)}{2(2J+1)(2J+3)}\,\frac{(E-\Delta E_J)^{1/2}}{(E-\Delta E_0)^{1/2}}\,\sigma(0\to2), \tag{18}$$

where $\Delta E_J=E_{J+2}-E_J$ is the excitation energy in the transition from J to $J+2$. This scaling law was first derived from the Born approximation with a simple long-range charge-quadrupole interaction [29]. However, it also follows more generally from the adiabatic approximation [as shown by Shimamura [30], provided that $\sigma(0\to2)$ is much larger than $\sigma(0\to0)$ or $\sigma(0\to J)$ with $J\geqslant4$].

The present cross-section data are discussed in detail in Refs. [27,28]. We provide some quantitative descriptions of the cross-section data. The vibrationally inelastic cross section for $V=0$ to 1 above 1.5 eV and $V=0$ to 2 are consistent with those of Ehrhardt *et al.* [31] and with those evaluated by Tawara *et al.* [32]. The rotationally inelastic cross sections for $J=0$ to 2 and $J=1$ to 3 show a good agreement with those evaluated by Tawara *et al.* [32]. The momentum transfer cross section of Buckman and Phelps [27] agrees very closely with that of England *et al.* [28] below 2 eV within $\pm0.63\%$. The momentum transfer cross section in the low energy region is important to the present study. The momentum transfer cross section of Buckman and Phelps becomes smaller and smaller than that of England *et al.* with increasing energy up to 10 eV. The momentum transfer cross section of England *et al.* is larger than that of Buckman and Phelps by 5.6% at 3 eV and by 14.7% at 6 eV.

We calculate the energy level with a rotational quantum number J and vibrational quantum number V with the equation

$$E_{JV}=B_VJ(J+1)-D_VJ^2(J+1)^2, \tag{19}$$

where $B_V=B_e-\alpha_e(V+\frac{1}{2})$ and $D_V=D_e-\beta_e(V+\frac{1}{2})$. The constants in B_V and D_V are taken from Ref. [33]. We use Eq. (19) to calculate the population density of the rotational levels with $V=0$ and to obtain the rotational threshold energies for $J=4$ to 6, 5 to 7, and 6 to 8. We use the rotational threshold energies given by England *et al.* for their cross sections. The threshold energies obtained from Eq. (19) and those of England *et al.* are virtually the same, the differences being about one in the fourth digit.

We can understand which collision process is dominant in terms of energy loss by using the stopping cross section. Figure 1(B) shows the stopping cross section $s(E)$. The stopping cross section can be obtained with Eq. (15) including the momentum transfer process and inelastic processes for $V=0$ to 1, $V=0$ to 2, and $J=0$ to 2 in the right-hand side of the equation. Each stopping cross section for the included processes is also shown in Fig. 1(B). The product of N_b and $s(E)$ is the stopping power, and the reciprocal of the stopping power is the cumulative degradation spectrum with the CGA and CSDA at $t=\infty$ as shown in Ref. [2].

It is also useful to point out that we use the microscopic reversibility relation

$$\xi_iE\sigma_{ij}(E)=\xi_j(E-E_{ij})\sigma_{ji}(E-E_{ij}), \tag{20}$$

TABLE I. Time steps in time intervals used in the present calculations for initial energies of 1, 3, and 5 eV. The symbol Δt represents a time step.

E_0	1 eV, 3 eV											
t (ns)	0		8×10^{-5}		4×10^{-4}		0.65		1.0		6.0	
Δt (ns)		5×10^{-7}		1×10^{-5}		2×10^{-4}		5×10^{-4}		0.001		
E_0	5 eV											
t (ns)	0		8×10^{-5}		4×10^{-4}		0.05		0.65		1.0	6.0
Δt (ns)		5×10^{-7}		1×10^{-5}		1×10^{-4}		2×10^{-4}		5×10^{-4}	0.001	

where ξ_i and ξ_j are the degeneracies of molecular states i and j, respectively. For vibrational quantum states, ξ_i and ξ_j are the unit numbers.

IV. RESULTS AND DISCUSSIONS

We organize the present results and discussions as follows.

(1) The time evolution of the electron density distribution function with electron initial energies of 1, 3, and 5 eV.

(2) The time evolution of the cumulative degradation spectrum with the three initial energies.

(3) Time-dependent (cumulative) yields and G values for vibrational processes and rotational processes.

(4) Thermalization times obtained from the Boltzmann equation and the CSDA.

A. Numerical calculation

We calculate the time evolution of the electron energy distribution function by using Eq. (9), and that of the cumulative degradation spectrum by using Eq. (10). The reason we use Eq. (10) instead of Eq. (11) in order to obtain the time evolution of the cumulative degradation spectrum is as follows. If we use Eq. (11), the successive over-relaxation (SOR) method requires many more iteration times than using Eq. (10) in a long time range because the cumulative degradation spectrum increases around the thermal energy with time. On the other hand, the iteration time of the SOR method decreases with time in the long time range because the electron energy distribution function is becoming close to the thermal distribution in that time range. Furthermore, if we use Eq. (10), we can obtain the cumulative degradation spectrum as well as the electron energy distribution function at almost the same cost as obtaining the electron energy distribution function. A shortcoming of using Eq. (10) is that we need a finer time step in a short time range than Eq. (11). A time step of 0.0002 ns is not appropriate for calculating the cumulative degradation spectrum with Eq. (10), but is enough for the electron energy distribution function. The time step of 0.0002 ns gives a misleadingly high value of the cumulative degradation spectrum at the source energy in using Eq. (10) although this cumulative degradation spectrum is not bad as a weak solution for calculating the yields by use of Eq. (12).

We choose 1, 3, and 5 eV as electron initial energies. We use the same energy mesh and time steps for calculating the electron distribution function and cumulative degradation spectrum. The energy mesh of 0.0005 eV is used in the whole time range for the three different energies. We carry out the calculations by dividing the whole time range into time intervals for each of the initial energies, and we use different time steps in the time intervals. Table I exhibits the time steps in the time intervals used for the present calculations. For the initial energy of 1 eV, we carry out calculations in an energy range between 0 and 2 eV until the time reaches 1.0 ns. Then we carry out calculations in an energy range between 0 and 1 eV by using a time step of 0.001 ns until the terminal time of 6 ns. We carry out calculations in an energy range between 0 and 4 eV until 0.45 ns, in that between 0 and 2 eV until 1 ns, and in that between 0 and 1 eV until 6 eV. For the initial energy of 5 eV, we carry out calculations in an energy range between 0 and 6 eV from the beginning until 0.25 ns, in that between 0 and 4 eV until 0.45 ns, in that between 0 and 2 eV until 1.0 ns, and in that between 0 and 1 eV until 6 ns. The present calculations are conducted for H_2 gas at the number density of 2.69×10^{19} cm^{-3} and temperature of 300 K.

B. The time evolution of the electron energy distribution function

Figure 2 shows the time evolution of the function with the initial energy of 1 eV. As shown in Fig. 2(A), the initial electron distribution decreases rapidly with time in quite early times, and no other structures of the function are discernible. In the next time range shown in Fig. 2(B), the function at the source energy continues decreasing with time, and its width becomes greater because of elastic collisions as discussed in Ref. [2]. Two tiny spikes below 1 eV and one below 0.5 eV are appreciable in Fig. 2(B). The energy difference of the first spike below 1 eV to 1 eV matches the excitation energy with $J=0$ to 2, and that of the second spike below 1 eV to 1 eV matches the excitation energy with $J=1$ to 3. The energy difference of the spike below 0.5 eV to 1 eV matches the vibrational threshold energy with $V=0$ to 1. As seen in Fig. 2(C), the spikes due to rotational collisions below 1 eV become no longer isolated by 0.0012 ns. In Fig. 2(D), the peak of the function at 1 eV still decreases with time, shifting the position of the peak to lower energies. The peak below 1 eV due to rotational collisions with $J=1$ to 3 becomes a shoulder by 0.008 ns. The function around 1 eV has a long tail down to 0.7 eV, and other rotational collision processes included in the present calculations as well as those with $J=0$ to 2 and $J=1$ to 3 contribute to the formation of the long tail. Two isolated portions of the function increase with time. As is clear from Fig. 2(E), the isolated

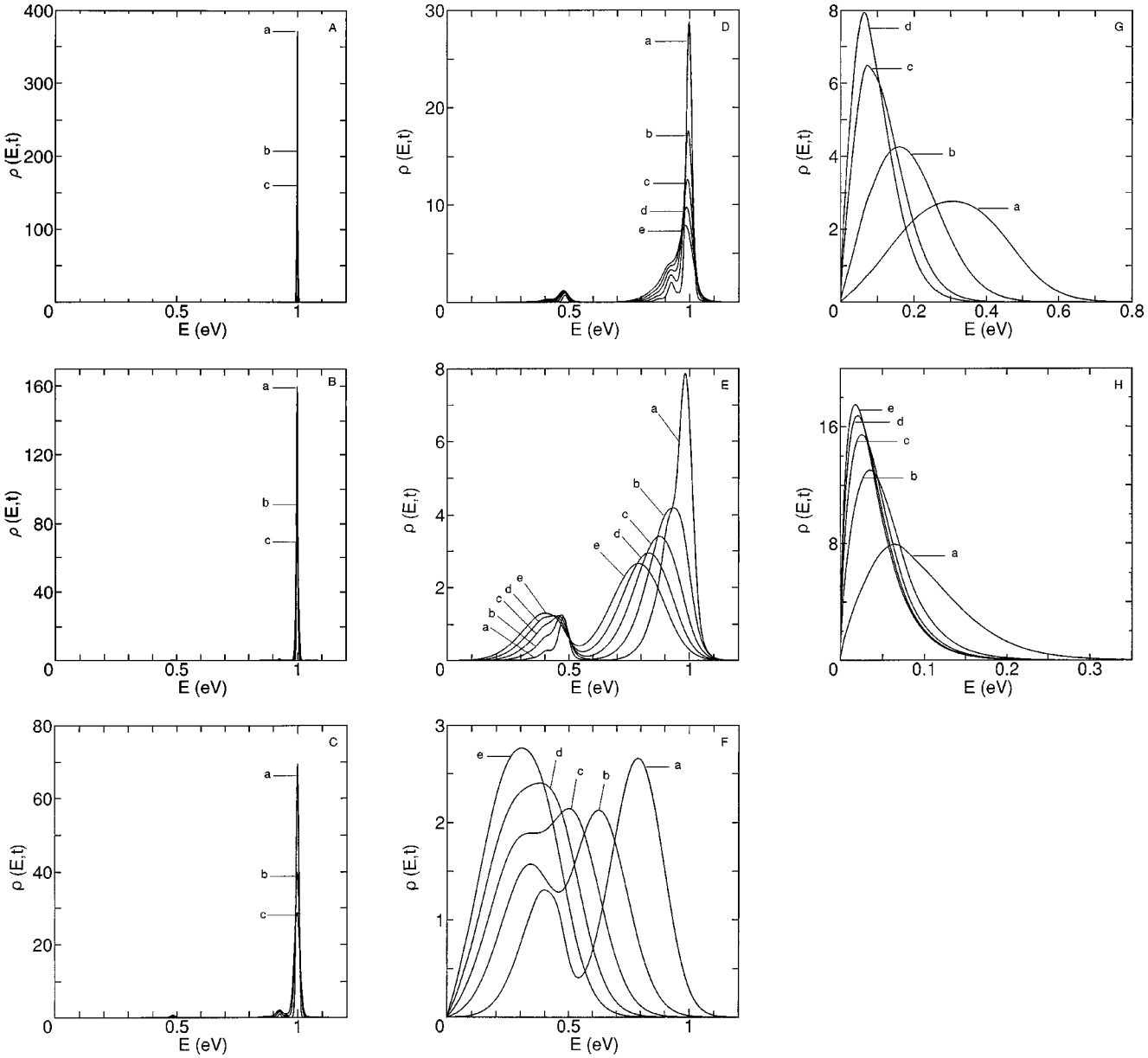

FIG. 2. Time evolution of the electron density distribution in H_2 at $T=$ 300 K. The initial δ function distribution is at 1 eV. The time in nanoseconds is equal to (A)—(a) 0.000 016, (b) 0.000 048, (c) 0.000 08; (B)—(a) 0.000 08, (b) 0.000 24, (c) 0.0004; (C)—(a) 0.0004, (b) 0.001, (c) 0.002; (D)—(a) 0.002, (b) 0.004, (c) 0.006, (d) 0.008, (e) 0.01; (E)—(a) 0.01, (b) 0.02, (c) 0.03, (d) 0.04, (e) 0.05; (F)—(a) 0.05, (b) 0.1, (c) 0.15, (d) 0.2, (e) 0.25; (G)—(a) 0.25, (b) 0.5, (c) 0.825, (d) 1; (H)—(a) 1, (b) 2, (c) 3, (d) 4, (e) 5. The unit of the vertical axis is 1/eV.

portion of the function around 1 eV and that around 0.5 eV shows a similarity that each shows a shoulder due to rotational collisions below each peak.

Because two times the vibrational threshold energy with $V=0$ to 1 is very close to the vibrational threshold energy with $V=0$ to 2, electrons at around the source energy suffering one vibrationally inelastic collision are also responsible for the second spike below the spike around the source energy, however; because the collision number of the vibrationally inelastic collisions with $V=0$ to 2 is much less than that with $V=0$ to 1, the contribution from the vibrationally inelastic collisions with $V=0$ to 2 to the second spike is very minor in comparison with that for the collisions with $V=0$ to 1. Two isolated parts are merging with time, and a shoulder of each peak is disappearing. The function shows two smooth peaks by 0.05 ns, shifting the two peaks to the lower energies. In Fig. 2(F), the function continues shifting the positions of the two peaks to the lower energies and forms a single peak by 0.2 ns. The single peak grows with time, shifting its position to the lower energies. In Figs. 2(G) and 2(H), the function shifts its peak to the lower energies as increasing the height of the peak. The function at later times shown in Fig. 2(H) becomes close to the thermal distribution.

Figures 3 and 4 show the time evolution of the function with the initial energies of 3 and 5 eV, respectively. The time evolution of the function before 0.0004 ns is not shown in Figs. 3 and 4 because it is similar to that for the initial energy of 1 eV shown in Figs. 2(A) and 2(B). The function in Fig. 3(A) shows three isolated spikes with a broad width due to rotational collisions. The spacing between two adjoining

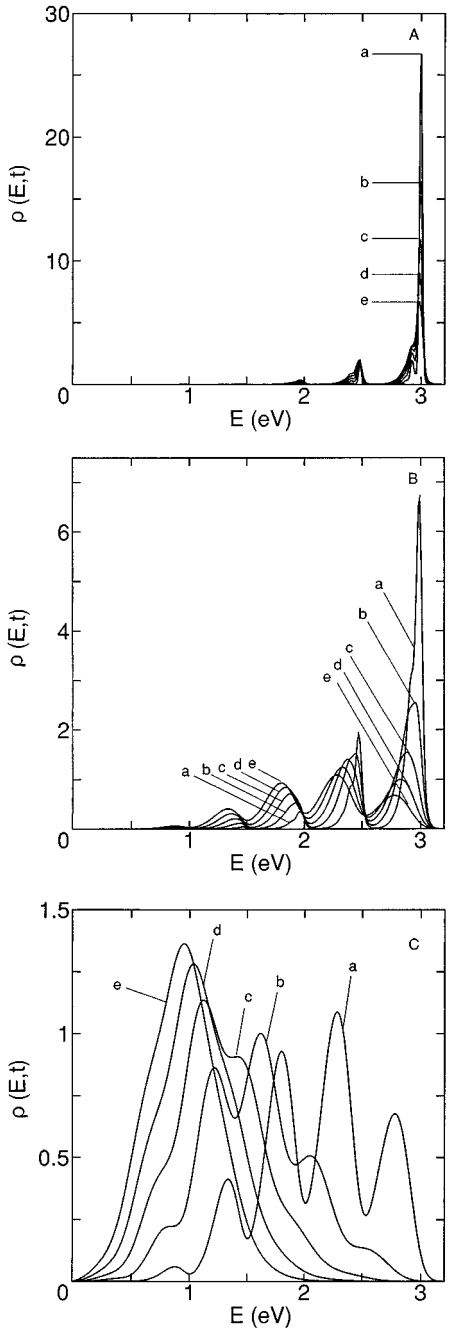

FIG. 3. Time evolution of the electron density distribution in H_2 at $T=$ 300 K. The initial δ function distribution is at 3 eV. The time in nanoseconds is equal to (A)—(a) 0.0004, (b) 0.0008, (c) 0.0012, (d) 0.0016, (e) 0.002; (B)—(a) 0.002, (b) 0.004, (c) 0.006, (d) 0.008, (e) 0.01; (C)—(a) 0.01, (b) 0.02, (c) 0.03, (d) 0.04, (e) 0.05. The unit of the vertical axis is 1/eV.

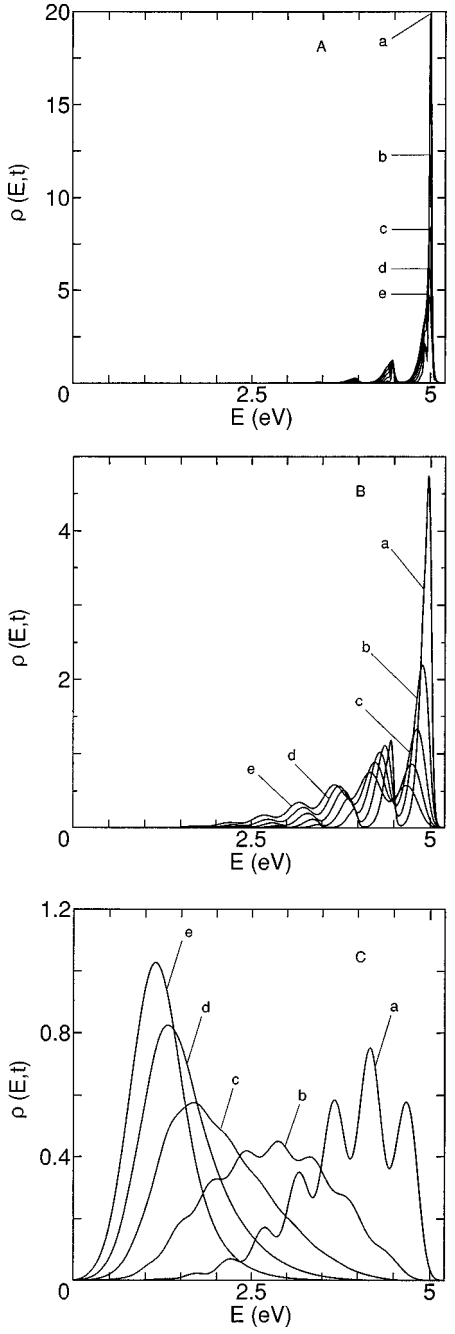

FIG. 4. Time evolution of the electron density distribution in H_2 at $T=$ 300 K. The initial δ function distribution is at 5 eV. The time in nanoseconds is equal to (A)—(a) 0.0004, (b) 0.0008, (c) 0.0012, (d) 0.0016, (e) 0.002; (B)—(a) 0.002, (b) 0.004, (c) 0.006, (d) 0.008, (e) 0.01; (C)—(a) 0.01, (b) 0.02, (c) 0.03, (d) 0.04, (e) 0.05. The unit of the vertical axis is 1/eV.

spikes matches the vibrational threshold energy with $V=0$ to 1 as is the case with the initial energy of 1 eV. Electrons at around the source energy suffering one vibrationally inelastic collision apart from rotationally inelastic collisions and elastic collisions are responsible for the first portion below the spike at around the source energy, and those suffering two vibrationally inelastic collisions with $V=0$ to 1 are primarily responsible for the second spike below the spike at around the source energy.

C. The time evolution of the cumulative degradation spectrum

Figure 5 shows the time evolution of the cumulative degradation spectrum with the initial energy of 1 eV. As shown in Fig. 5(A), the cumulative degradation spectrum at 0.0004 ns consists of two portions, that is, one around 1 eV and the other just below 0.5 eV. The cumulative degradation spectrum around 1 eV shows two isolated spikes above the source energy of 1 eV and four merging spikes below the source energy. The energy difference between the first spike

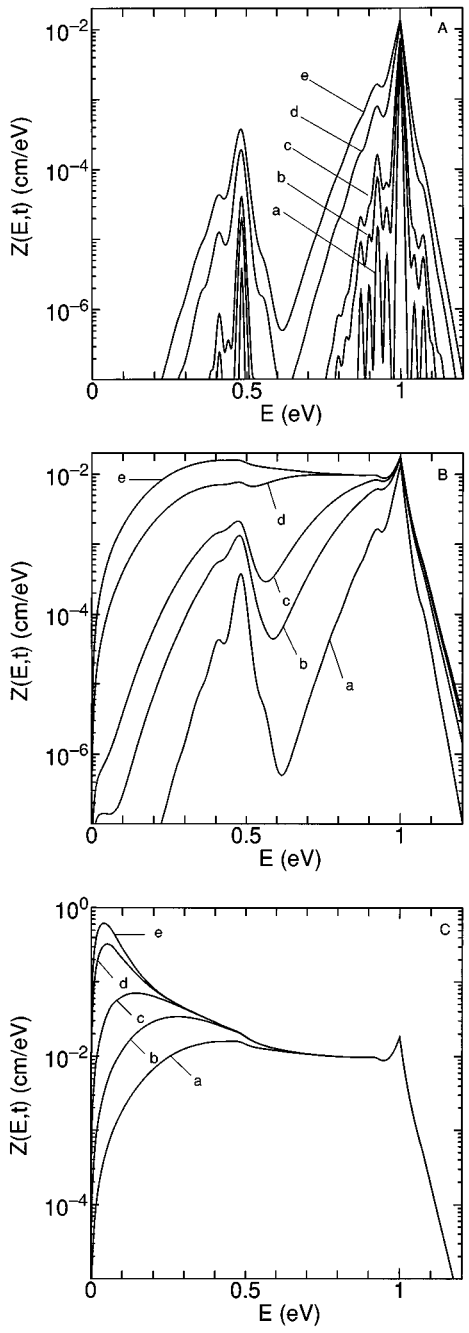

FIG. 5. Time evolution of the cumulative degradation spectrum in H_2 at $T=$ 300 K. The initial δ function distribution is at 1 eV. The time in nanoseconds is equal to (A)—(a) 0.0004, (b) 0.0012, (c) 0.002, (d) 0.006, (e) 0.01; (B)—(a) 0.01, (b) 0.03, (c) 0.05, (d) 0.15, (e) 0.25; (C)—(a) 0.25, (b) 0.5, (c) 1, (d) 3, (e) 5.

above 1 eV and 1 eV matches the rotational threshold energy for $J=0$ to 2, and that between the second spike above 1 eV and 1 eV matches the rotational threshold energy for $J=1$ to 3. The first spike above 1 eV arises from superelastic collisions due to rotational deexcitation with $J=2$ to 0, and the second spike above 1 eV is superelastic collisions due to rotational deexcitation with $J=3$ to 1. From the energy differences between each of four nonisolated spikes below 1 eV and 1 eV, it is considered that the first spike comes from rotationally inelastic collisions with $J=0$ to 2, the second spike from those with $J=1$ to 3, the third spike from those with $J=2$ to 4, and the fourth spike from those with $J=3$ to 5. The spike below 0.5 eV occurs because of vibrationally inelastic collisions with $V=0$ to 1, as we saw in the case of the electron energy distribution function.

The cumulative degradation spectrum grows with time, and the portion around 1 eV at 0.0012 ns shows overlapping structures above 1 eV as well as below 1 eV. Two additional peaks can be seen below 1 eV. From the energy differences between each of the additional peaks and 1 eV, the fifth peak is due to rotationally inelastic collisions with $J=4$ to 6, and the sixth is because of those with $J=5$ to 7. A shoulder at 1.1 eV appears by 0.0012 ns because of superelastic collisions due to rotational deexcitation with $J=4$ to 2. The cumulative degradation spectrum around 0.5 eV at 0.0012 ns shows an additional tiny spike. Two channels are responsible for the additional tiny spike below 0.5 eV. In the first channel, electrons at the source of 1 eV suffer one vibrationally inelastic collision with $V=0$ to 1 and then one rotationally inelastic collision with $J=1$ to 3. In the second channel, electrons at 1 eV suffer one rotationally inelastic collision with $J=1$ to 3 and then one vibrationally inelastic collision with $V=0$ to 1. The cumulative degradation at 0.002 ns around 0.5 eV shows three peaks, and the second peak in this portion occurs because of the combination of two kinds of inelastic collisions with $V=0$ to 1 and $J=0$ to 2 similar to the third peak with the combination of $V=0$ to 1 and $J=1$ to 3. The cumulative degradation spectrum becomes smoother and grows with time, and it exhibits two primary peaks around 1 eV and 0.5 eV of which each has a subsidiary peak due to rotational collisions with $J=1$ to 3.

Figure 5(B) shows the time evolution of the cumulative degradation spectrum in the next time range. The valley between the two primary peaks becomes shallower and shallower with time, and a primary peak around 0.5 eV becomes insignificant by 0.15 ns, and the valley disappears by 0.25 ns. The cumulative degradation spectrum above 0.75 eV at 0.25 ns is indistinguishable from that at 0.15 ns in the figure, meaning that the spectrum above 0.75 eV has reached the steady state by 0.15 ns. Figure 5(C) shows the time evolution of the cumulative spectrum in the latter times. The cumulative degradation spectrum above about 0.3 eV reaches the steady state by 1 ns. The cumulative spectrum around the thermal energy keeps growing with time because of approach to the Maxwellian distribution.

We now turn to the steady part of the cumulative degradation spectrum above 0.3 eV at 1 ns. The spectrum decreases in both directions of increasing energy and decreasing energy from the peak at the source energy of 1 eV. Superelastic collisions due to rotational deexcitation, as well as elastic collisions, contribute to the spectrum above 1 eV. The spectrum shows an abrupt decrease from the peak with decreasing energy and an insignificant peak that is a remnant of the peak due to rotationally inelastic collisions with $J=1$ to 3. Then the spectrum shows a gentle increase, a moderate increase below 0.6 eV, and also a turning point that is a remnant of the second primary peak.

D. Time-dependent (cumulative) yields and G values

Figure 6 shows the (time-dependent) cumulative yields for inelastic processes such as the vibrational excitation for V

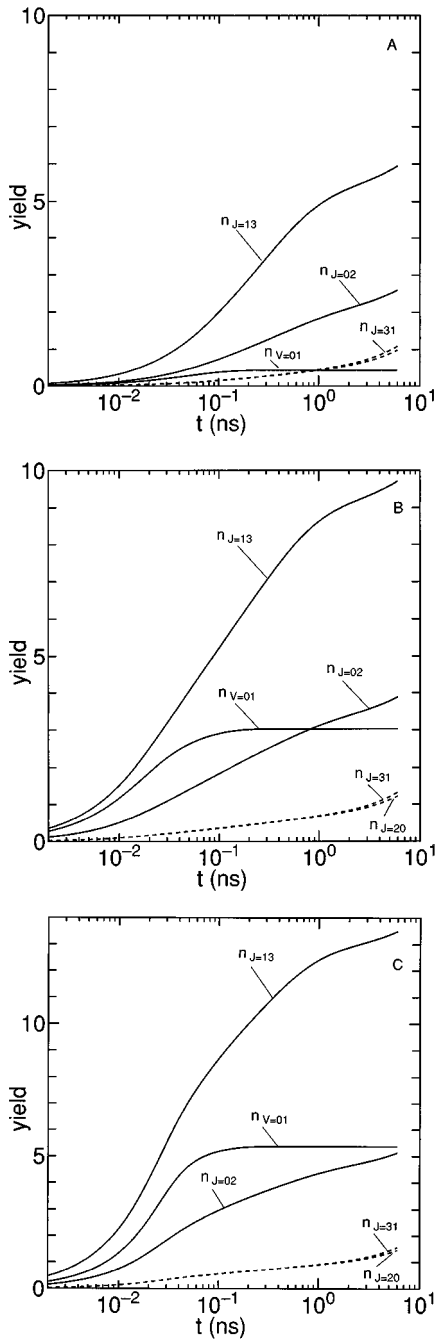

FIG. 6. The time-dependent cumulative collision numbers for $V=0$ to 1, $J=0$ to 2, $J=2$ to 0, $J=1$ to 3, and $J=3$ to 1. The initial electron energy in eV is equal to (A) 1, (B) 3, and (C) 5.

$=0$ to 1 and the rotational excitations for $J=0$ to 2 and $J=1$ to 3 with the initial energies of 1, 3, and 5 eV. The cumulative yields for the inverse processes of the inelastic processes are also included in Fig. 6.

Let us take a close look at common characteristics of the cumulative yields in the three different energies using Fig. 6(A). As is clear from Fig. 6(A), both cumulative yields for the rotational excitations for $J=0$ to 2 and 1 to 3 increase with time in the whole time region of the figure. This behavior is understandable because the cumulative degradation spectrum increases with time even when the electron distribution function is close to the thermal distribution. Although the cross section for $J=0$ to 2 is larger than that for $J=1$ to 3 as shown in Fig. 1, the cumulative yield for $J=1$ to 3 is several times larger than that for $J=0$ to 2. The total statistical weight for the state $J=1$ with $V=0$ of which total nuclear spin $I=1$ is nine times larger than that for the state $J=0$ with $V=0$ of which total nuclear spin $I=0$. The total statistical weight contributes the larger cumulative yield for $J=1$ to 3 than that for $J=0$ to 2. In Fig. 6(A), the dotted curves represent the cumulative yields for $J=2$ to 0 and $J=3$ to 1, and they are not separable until 1 ns. After 1 ns the cumulative yield for $J=3$ to 1 becomes larger than that for $J=2$ to 0. Both curves show an increase even in times close to thermalization, and the growth rate of the cumulative yield for $J=0$ to 2 closely matches that for $J=2$ to 0, and the same is true for those for $J=1$ to 3 and 3 to 1. So if we define a net yield for an inelastic process as the difference between the cumulative yield for the inelastic process and that for the inverse process, the net yield approaches a constant value with increasing time. The cumulative yield for $V=0$ to 1 reaches a plateau by 0.2 ns. Because the threshold energy for the vibrational excitation $V=0$ to 1 is much higher than the thermal energy, the contribution to the cumulative yield from the increase of the cumulative degradation spectrum is very small in the time range close to thermalization.

The tendency for each curve in Figs. 6(B) and 6(C) is similar to the corresponding one in Fig. 6(A). With increasing initial energy, the cumulative yield for the vibrational excitation $V=0$ to 1 becomes much larger than that for the rotational excitation $J=0$ to 2. The ratio of the cumulative yield for the vibrational excitation $V=0$ to 1 to that for the rotational excitation for $J=1$ to 3 becomes larger with increasing initial energy. This means that the vibrationally inelastic process becomes more significant with increasing initial energy. This is seen particularly clearly in the cumulative degradation spectrum.

If we use Eq. (12) and the definition of the net yield, a net cumulative yield $\tilde{n}_{lm}$ for an inelastic process lm can be written as

$$\tilde{n}_{lm}(t)=n_{lm}(t)-n_{ml}(t). \tag{21}$$

We show the net cumulative yields for the rotational and vibrational yields involved in the present calculations with the initial energies of 1, 3, and 5 eV in Table II. Each net cumulative yield shown in Table II exhibits an increase with increasing time and convergence in a long time range. The net cumulative yield for each process increases with increasing initial energy at the same time except for that for $V=0$ to 1 in earlier times. The net yield for $V=0$ to 1 with the initial energy of 3 eV is larger than that with the initial energy of 1 eV in earlier times, but smaller than that with the initial energy of 5 eV until 0.002 ns. Because most of the electrons are distributed around an initial energy at earlier times, as seen in Figs. 2–4, each net cumulative yield is roughly proportional to the product of the corresponding cross section at the initial energy E_0 and the speed $\sqrt{(2E_0/m)}$. As is clear from Fig. 1, the cross section for $V=0$ to 1 shows a steep decrease with increasing energy above its peak at 3 eV. The steep decrease of the cross section between 3 and 5 eV overwhelms the increase of the initial speed.

Even when the initial energy is 1 eV, the net cumulative yield for $V=0$ to 2 with the threshold energy of 1 eV is not

TABLE II. Net cumulative yields for vibrational and rotational excitations in H_2 at a temperature of 300 K and the number density of $2.69\times10^{19}cm^{-3}$ for initial energies of 1, 3, and 5 eV. Numbers enclosed in brackets indicate powers of 10.

			E_0=1 eV		
t (ns)	$J=0\rightarrow2$	$J=1\rightarrow3$	$J=2\rightarrow4$	$J=3\rightarrow5$	$J=4\rightarrow6$
0.001	0.1034[−1]	0.3212[−1]	0.4823[−2]	0.3896[−2]	0.1838[−3]
0.002	0.2050[−1]	0.6375[−1]	0.9566[−2]	0.7726[−2]	0.3645[−3]
0.005	0.5004[−1]	0.1557	0.2333[−1]	0.1884[−1]	0.8891[−3]
0.01	0.9625[−1]	0.3002	0.4485[−1]	0.3618[−1]	0.1709[−2]
0.02	0.1789	0.5599	0.8326[−1]	0.6708[−1]	0.3171[−2]
0.05	0.3699	1.169	0.1720	0.1379	0.6525[−2]
0.1	0.5797	1.851	0.2697	0.2146	0.1013[−1]
0.2	0.8277	2.673	0.3858	0.3039	0.1420[−1]
0.5	1.173	3.805	0.5439	0.4198	0.1894[−1]
1.0	1.399	4.448	0.6201	0.4685	0.2058[−1]
2.0	1.539	4.750	0.6439	0.4807	0.2094[−1]
5.0	1.607	4.851	0.6490	0.4830	0.2111[−1]
6.0	1.612	4.857	0.6493	0.4831	0.2115[−1]

$J=5\rightarrow7$	$J=6\rightarrow8$	$V=0\rightarrow1$	$V=0\rightarrow2$
0.4169[−4]	0.6303[−6]	0.9445[−2]	0.5200[−6]
0.8268[−4]	0.1250[−5]	0.1865[−1]	0.1369[−5]
0.2016[−3]	0.3048[−5]	0.4492[−1]	0.4546[−5]
0.3874[−3]	0.5854[−5]	0.8460[−1]	0.9987[−5]
0.7183[−3]	0.1085[−4]	0.1511	0.1829[−4]
0.1475[−2]	0.2222[−4]	0.2809	0.2757[−4]
0.2282[−2]	0.3426[−4]	0.3783	0.2939[−4]
0.3178[−2]	0.4734[−4]	0.4261	0.2950[−4]
0.4158[−2]	0.6058[−4]	0.4327	0.2950[−4]
0.4442[−2]	0.6357[−4]	0.4328	0.2950[−4]
0.4487[−2]	0.6392[−4]	0.4328	0.2950[−4]
0.4493[−2]	0.6396[−4]	0.4328	0.2950[−4]
0.4493[−2]	0.6396[−4]	0.4328	0.2950[−4]

			E_0=3 eV		
t (ns)	$J=0\rightarrow2$	$J=1\rightarrow3$	$J=2\rightarrow4$	$J=3\rightarrow5$	$J=4\rightarrow6$
0.001	0.4838[−1]	0.1689	0.2422[−1]	0.1978[−1]	0.8804[−3]
0.002	0.9515[−1]	0.3318	0.4761[−1]	0.3888[−1]	0.1731[−2]
0.005	0.2257	0.7847	0.1128	0.9212[−1]	0.4103[−2]
0.01	0.4121	1.424	0.2058	0.1680	0.7485[−2]
0.02	0.6897	2.354	0.3434	0.2802	0.1251[−1]
0.05	1.135	3.784	0.5600	0.4563	0.2051[−1]
0.1	1.476	4.870	0.7203	0.5845	0.2652[−1]
0.2	1.800	5.932	0.8714	0.7022	0.3199[−1]
0.5	2.195	7.235	1.054	0.8380	0.3767[−1]
1.0	2.439	7.943	1.140	0.8938	0.3958[−1]
2.0	2.587	8.267	1.167	0.9074	0.3998[−1]
5.0	2.658	8.373	1.172	0.9098	0.4015[−1]
6.0	2.663	8.379	1.172	0.9099	0.4019[−1]

$J=5\rightarrow7$	$J=6\rightarrow8$	$V=0\rightarrow1$	$V=0\rightarrow2$
0.2019[−3]	0.3082[−5]	0.1389	0.9652[−2]
0.3969[−3]	0.6059[−5]	0.2736	0.1871[−1]
0.9405[−3]	0.1436[−4]	0.6495	0.4225[−1]
0.1715[−2]	0.2617[−4]	1.173	0.7032[−1]
0.2863[−2]	0.4365[−4]	1.870	0.9787[−1]
0.4686[−2]	0.7131[−4]	2.621	0.1124

TABLE II. (*Continued*).

	$J=5\rightarrow7$	$J=6\rightarrow8$	$V=0\rightarrow1$	$V=0\rightarrow2$	
	0.6043[−2]	0.9174[−4]	2.903	0.1134	
	0.7258[−2]	0.1097[−3]	3.012	0.1134	
	0.8453[−2]	0.1262[−3]	3.027	0.1134	
	0.8791[−2]	0.1299[−3]	3.027	0.1134	
	0.8842[−2]	0.1303[−3]	3.027	0.1134	
	0.8848[−2]	0.1303[−3]	3.027	0.1134	
	0.8849[−2]	0.1303[−3]	3.027	0.1134	
			$E_0=5$ eV		
t (ns)	$J=0\rightarrow2$	$J=1\rightarrow3$	$J=2\rightarrow4$	$J=3\rightarrow5$	$J=4\rightarrow6$
0.001	0.6308[−1]	0.2215	0.3159[−1]	0.2582[−1]	0.1154[−2]
0.002	0.1257	0.4415	0.6294[−1]	0.5147[−1]	0.2299[−2]
0.005	0.3102	1.090	0.1554	0.1270	0.5671[−2]
0.01	0.6030	2.119	0.3019	0.2469	0.1102[−1]
0.02	1.107	3.877	0.5537	0.4525	0.2019[−1]
0.05	1.927	6.635	0.9598	0.7837	0.3504[−1]
0.1	2.397	8.133	1.184	0.9646	0.4341[−1]
0.2	2.773	9.357	1.359	1.102	0.4983[−1]
0.5	3.194	10.75	1.556	1.248	0.5602[−1]
1.0	3.447	11.49	1.646	1.308	0.5807[−1]
2.0	3.600	11.83	1.674	1.322	0.5849[−1]
5.0	3.671	11.93	1.679	1.324	0.5867[−1]
6.0	3.676	11.94	1.679	1.325	0.5871[−1]
	$J=5\rightarrow7$	$J=6\rightarrow8$	$V=0\rightarrow1$	$V=0\rightarrow2$	
	0.2650[−3]	0.4053[−5]	0.1291	0.1252[−1]	
	0.5280[−3]	0.8075[−5]	0.2595	0.2502[−1]	
	0.1303[−2]	0.1992[−4]	0.6587	0.6219[−1]	
	0.2530[−2]	0.3868[−4]	1.340	0.1215	
	0.4635[−2]	0.7083[−4]	2.635	0.2182	
	0.8030[−2]	0.1225[−3]	4.621	0.3128	
	0.9929[−2]	0.1512[−3]	5.179	0.3193	
	0.1136[−1]	0.1726[−3]	5.341	0.3194	
	0.1267[−1]	0.1908[−3]	5.363	0.3194	
	0.1304[−1]	0.1948[−3]	5.364	0.3194	
	0.1309[−1]	0.1952[−3]	5.364	0.3194	
	0.1310[−1]	0.1953[−3]	5.364	0.3194	
	0.1310[−1]	0.1953[−3]	5.364	0.3194	

null, as shown in Table II. This is because electrons with energies greater than the initial energy of 1 eV are generated owing to superelastic collisions due to rotational deexcitation and to elastic collisions.

Kimura, Krajar-Bronić, and Inokuti [16] reported that the ratio 2.8 of the yield for $J=1$ to 3 to that for $J=0$ to 2 at 0 °C with the initial energy of 8 eV is consistent with that of Douthat [34] at 23 °C with the subexcitation spectrum generated from the initial electron energy of 10 keV. Our present result averaged over the initial energies of 1, 3, and 5 eV gives the ratio of 3.14 which agrees with the previous result of 2.8 within 11%. Douthat obtained yields for the other rotational processes such as $J=2$ to 4, $J=3$ to 5, and $J=4$ to 6. The ratios of the yields for $J=2$ to 4, $J=3$ to 5, and $J=4$ to 6 averaged over the three initial energies are in agreement with those of Douthat within 15%, 36%, and 56%, respectively. Douthat used the CSDA and did not include energy gain from H_2. Our initial electron distribution is different from that of Douthat as described previously. In spite of all these differences, the agreement of ours with Douthat's in the ratios of the rotational yields is reasonable.

The G value, that is, the number of a product species generated per absorbed energy of 100 eV, is commonly used in radiation chemistry. The G value for an inelastic process lm is given as

$$G_{lm}=\frac{100}{E_Q}\tilde{n}_{lm}, \tag{22}$$

where E_Q is an absorbed energy. We assume initial energy is absorbed to H_2 at 6 ns. Using Eq. (22), we present G values for $J=0$ to 2, $J=1$ to 3, $J=2$ to 4, $J=3$ to 5, $J=4$ to 6, $J=5$ to 7, $J=6$ to 8, $V=0$ to 1, and $V=0$ to 2 in Table III. Table III shows that the G values for all rotationally inelastic processes decrease with increasing initial energy and that those for the two vibrationally inelastic processes increase. As initial energy increases, the decrease or increase of each G value becomes gradual.

E. Thermalization times

Figure 7 shows thermalization times with the initial energies of 1, 3, and 5 eV. The solid curves represent the thermalization times which are the changes of the average energy of electrons obtained from Eq. (17), and the dotted curves express the CSDA times obtained from Eq. (16). The thermalization time and CSDA time show a moderate agreement on the whole in every case given in Fig. 7. They agree very well in a short time range and deviate in a long time range. To derive Eq. (15), we apply the CGA as well as the CSDA. Then the CSDA time reaches the electron energy of 0 eV, while the average energy obtained from Eq. (17) reaches the thermal energy. When we calculate the stopping power, we use an approximation that the stopping cross section for rotational excitation is that for $J=0$ to 2 only. The stopping cross section for rotational excitation corresponds to an appreciable part of the total stopping cross section, and the thermal distribution of the rotational states spreads over many rotational quantum numbers. As shown by Shimamura [35], the stopping cross section for rotational excitation with the thermal distribution can be approximated as the stopping cross section for $J=0$ to 2 if the cross sections $\sigma(0\rightarrow J)$ with $J\geqslant 4$ are much smaller than $\sigma(0\rightarrow 2)$, which is indeed the case with electron scattering by H_2. The overall agreement between the thermalization time and the CSDA time means that the stopping power is obtained with a good approximation, that is, the approximation of rotational stopping cross section with $J=0$ to 2 only is good.

The thermalization time $\tau_{1.1}$ is defined as the time that the average energy of electrons reaches an energy 1.1 times larger than the thermal energy. Similarly, we define $\tau_{1.05}$ as the time in which the average energy of electrons reaches an energy 1.05 times larger than the thermal energy. Table IV shows the thermalization times $\tau_{1.1}$ and $\tau_{1.05}$. The thermalization times $\tau_{1.1}$ and $\tau_{1.05}$ obtained from Eq. (17) increase with increasing initial energy, and the CSDA times for $\tau_{1.1}$ and $\tau_{1.05}$ show the same behavior with increasing energy. Koura [22] reported thermalization times $\tau_{1.1}$ with some initial energies in H_2 by using the Monte Carlo study, and $\tau_{1.1}=4.1$ ns at 300 K with the initial energy of 10 000 K (1.29 eV) is given. This agrees closely with the present result of 4.2 ns shown in Table IV. However, Koura's $\tau_{1.1}$ with the initial energy of 30 000 K is 3.8 ns, and the thermalization times are not in order with increasing initial energy. Table IV shows that the thermalization times $\tau_{1.1}$ increase with increasing initial energy. As shown in Figs. 3 and 4, the electron distribution functions with the initial energies of 3 and 5 eV become smooth curves with one peak by 0.05 ns, at which time the average energies of both exceed 1 eV slightly, as is seen in Fig. 7. It takes some further time until the

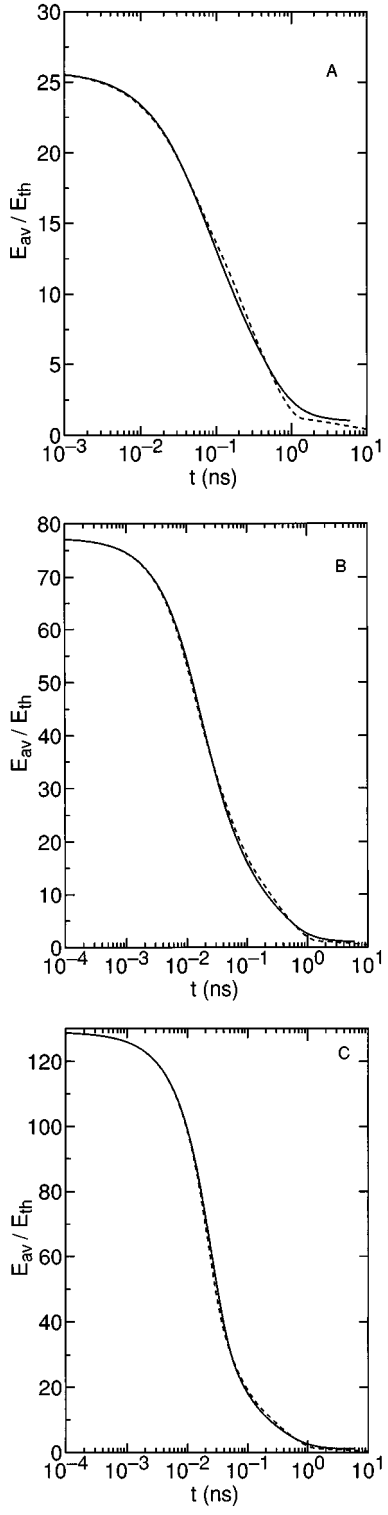

FIG. 7. The thermalization of the average electron energy in H_2 at 300 K; the initial electron energy in eV is equal to (A) 1, (B) 3, and (C) 5. The dashed curve is the CSDA time.

average energy of electrons with an initial energy E_A reaches some lower energy corresponding to the other initial energy E_B. The electron distribution function with the initial energy E_A after some time when the average energy of electrons reaches E_B generally differs from a δ function as the initial distribution function with the initial energy E_A. In our calculations, the time in which E_{av}/E_{th} reaches 1.1 using the

TABLE III. G values for vibrational and rotational excitations in H_2 at a temperature of 300 K and the number density of 2.69×10^{19} cm^{-3} for initial energies of 1, 3, and 5 eV. Numbers enclosed in brackets indicate powers of 10.

E_0 (eV)	$J=0\rightarrow2$	$J=1\rightarrow3$	$J=2\rightarrow4$	$J=3\rightarrow5$	$J=4\rightarrow6$
1	161.0	486.0	64.9	48.3	2.11
3	88.8	279.0	39.1	30.3	1.34
5	73.5	239.0	33.6	26.5	1.17

	$J=5\rightarrow7$	$J=6\rightarrow8$	$V=0\rightarrow1$	$V=0\rightarrow2$
	0.449	0.640[−2]	43.3	0.295[−2]
	0.295	0.434[−2]	101.0	3.78
	0.262	0.391[−2]	107.0	6.39

distribution function with the initial energy of 3 or 5 eV at 0.05 ns as an initial distribution function with the initial energy of 1 eV amounts to the thermalization time $\tau_{1.1}$ with the initial energy of 1 eV. This means that the thermalization time $\tau_{1.1}$ is insensitive to the initial distribution function. Koura [22] reports that the thermalization time $\tau_{1.1}$ with the initial energy of 30 000 K was shorter than that with the initial energy of 10 000 K; however, it is considered that the fluctuation of the Monte Carlo calculations caused this.

Warman and Sauer [19] gave the thermalization time $\tau_{1.1}$ in H_2 from $E_{av}/E_{th}=25$ to $E_{av}/E_{th}=1.1$ as $\tau_{1.1}=1.85$ ns at the number density of 2.69×10^{19} cm^{-3} and at 296 K. This value is much shorter than the present $\tau_{1.1}$ with the initial energy of 1 eV shown in Table IV but close to the $\tau_{1.1}$ of the CSDA time. It is probably not a good approximation to assume that the average energy of electrons decays exponentially with only one exponential component from a high energy to a low energy close to thermal. It seems to require at least several exponential components to express the decay of the average energy of electrons with time. Indeed, Shizgal and McMahon [4] have shown that the decay is expressed as a sum of exponential functions with decay constants of eigenvalues in the case of elastic collisions only using the QDM. We obtain $E_{av}/E_{th}=2.53$ at 1 ns from the present calculations as the average value with the three different initial energies. The value of 2.53 at 300 K is converted to that of 2.56 at 296 K. If we assume that the thermalization constants given by Warman and Sauer express the decay of the average energy of electrons in the energy region between $E_{av}/E_{th}=25$ and $E_{av}/E_{th}=2.56$, we obtain the thermalization time of 0.92 ns, which is in good agreement with our thermalization time of 1 ns in the energy region between 1 and 0.095 eV. This is consistent with what Douthat [24] has pointed out.

Okigaki *et al.* [21] measured the thermalization time in H_2 on the basis of their observation that the average energy of electrons decays exponentially with time in the energy region close to the thermal energy. The thermalization time they report is the decay constant of the exponential function. Because the definition of the thermalization time of Okigaki *et al.* is different from that of the present study, we estimate the thermalization time $\tau_{1.1}$ from the data of Okigaki *et al.* In our understanding Okigaki *et al.* have measured the decay constants of microwave absorption signals in the energy region between about $E_{av}/E_{th}=2.5$ and 1.1. The time that electrons thermalize from 2.56 to 1.1 is evaluated as 3.4 ns using the data of Okigaki *et al.* Therefore we adopt 4.3 ns as the experimental $\tau_{1.1}$ derived from a combination of the results of Warman and Sauer [19] and Okigaki *et al.* [21]. The experimental $\tau_{1.1}$ shows a good agreement with our results. We can also evaluate the experimental $\tau_{1.05}$ from the data of Warman and Sauer and Okigaki *et al.* with the same way as used for $\tau_{1.1}$, and we obtain $\tau_{1.05}=5.1$ ns. Our $\tau_{1.05}$ is 5.7 ns on the average of the initial energies from Table IV, and the agreement between the experimental $\tau_{1.05}$ and our $\tau_{1.05}$ is not as good as that between the $\tau_{1.1}$'s.

V. SUMMARY

We have shown the time evolutions of the electron density distribution function with the initial energies of 1, 3, and 5 eV. We have presented the time evolution of the cumulative degradation spectrum with the initial energy of 1 eV.

We have calculated the cumulative yields or collision numbers for vibrational and rotational excitation processes and deexcitation processes. We have introduced the definition of a net yield as the difference of yields for an inelastic excitation process and the deexcitation process. Each net yield reaches a plateau in the long time range when the electron density distribution function approaches the thermal distribution. This shows the accuracies of the present calculation method. We have presented the G values for the vibrational and rotational processes. The net yields and G values provided here can be compared with experiments.

We have obtained the electron thermalization times in

TABLE IV. Thermalization times $\tau_{1.1}$ and $\tau_{1.05}$ for electrons in H_2.

E_0 (eV)	$\tau_{1.1}$[a]	$\tau_{1.05}$[a]	$\tau_{1.1}$[b]	$\tau_{1.05}$[b]
1.0	4.189	5.687	1.6870	1.9809
3.0	4.227	5.724	1.7357	2.0295
5.0	4.244	5.741	1.7607	2.0545

[a]Relaxation time in ns for E_{avg}/E_{th} to equal 1.1 or 1.05 as calculated from time-dependent solutions of Eq. (9), the Boltzmann equation; E_0 is the energy of the initial δ function distribution.
[b]Calculated from Eq. (16).

H_2 with the initial energies of 1, 3, and 5 eV. We have discussed our thermalization times with the experimental thermalization time derived from a combination of the results of Warman and Sauer [19] and Okigaki *et al.* [21]. Our theoretical $\tau_{1.1}$ is in good agreement with the experimental $\tau_{1.1}$. Our $\tau_{1.1}$ on the average of the initial energies is consistent with that of Koura [22]; however, the initial energy dependence of our $\tau_{1.1}$ is inconsistent with Koura's. It is concluded that the cause of the inconsistency arises from the fluctuation of Monte Carlo calculations. We have shown that the present method based on the numerical analysis of the Boltzmann equation has an advantage over the Monte Carlo method.

ACKNOWLEDGMENTS

The author thanks Dr. I. Shimamura and Dr. M. Inokuti for making constructive criticisms on an earlier version of the manuscript. The author acknowledges the encouragement of Dr. Y. Awaya. The present calculations were conducted with the RIKEN computer facilities supported by the RIKEN computer center.

[1] R. L. Platzman, Radiat. Res. **2**, 1 (1955).
[2] K. Kowari, L. Demeio, and B. Shizgal, J. Chem. Phys. **97**, 2061 (1992).
[3] K. Kowari and B. Shizgal, Chem. Phys. **185**, 1 (1994).
[4] B. Shizgal and D. R. A. McMahon, J. Phys. Chem. **88**, 4854 (1984).
[5] D. R. A. McMahon and B. Shizgal, Phys. Rev. A **31**, 1894 (1985).
[6] L. A. Viehland, S. Ranganathan, and B. Shizgal, J. Chem. Phys. **88**, 362 (1988).
[7] B. Shizgal, D. R. A. McMahon, and L. A. Viehland, Radiat. Phys. Chem. **34**, 35 (1989).
[8] B. Shizgal and T. Nishigori, Chem. Phys. Lett. **171**, 493 (1990).
[9] B. Shizgal, Can. J. Phys. **68**, 1213 (1990).
[10] B. Shizgal and L. Demeio, Can. J. Phys. **69**, 712 (1991).
[11] T. Nishigori, Chem. Phys. Lett. **221**, 492 (1994).
[12] L. V. Spencer and U. Fano, Phys. Rev. **93**, 1172 (1954).
[13] K. Kowari, M. Kimura, and M. Inokuti, J. Chem. Phys. **89**, 7229 (1988).
[14] M. A. Ishii, M. Kimura, M. Inokuti, and K. Kowari, J. Chem. Phys. **90**, 3081 (1989).
[15] M. A. Ishii, M. Kimura, and M. Inokuti, Phys. Rev. A **42**, 6486 (1990).
[16] M. Kimura, I. Krajar-Bronić, and M. Inokuti, J. Chem. Phys. **94**, 8244 (1991).
[17] M. Kimura, M. A. Dillon, and M. Inokuti, Adv. Chem. Phys. **84**, 193 (1993).
[18] K. Kowari, Radiat. Chem. **54**, 20 (1992).
[19] J. M. Warman and M. C. Sauer, Jr., J. Chem. Phys. **62**, 1971 (1975).
[20] E. Suzuki and Y. Hatano, J. Chem. Phys. **84**, 4915 (1986).
[21] S. Okigaki, E. Suzuki, K. Hayashi, K. Kurashige, and Y. Hatano, J. Chem. Phys. **96**, 8324 (1992).
[22] K. Koura, J. Chem. Phys. **80**, 5799 (1984).
[23] K. Koura, J. Phys. Soc. Jpn. **53**, 4192 (1984).
[24] D. A. Douthat, J. Chem. Phys. **79**, 4599 (1983).
[25] J. A. Stephens and F. Robicheaux, Radiat. Res. **110**, 19 (1987).
[26] D. A. Douthat, Astrophys. J. **314**, 419 (1987).
[27] S. J. Buckman and A. V. Phelps, J. Chem. Phys. **82**, 4999 (1985); JILA Information Center Report No. 27, 1985 (unpublished).
[28] J. T. England, L. P. Elford, and R. W. Crompton, Aust. J. Phys. **41**, 573 (1988).
[29] E. Gerjouy and S. Stein, Phys. Rev. **97**, 1671 (1955).
[30] I. Shimamura, in *Electron-Molecule Collisions*, edited by I. Shimamura and K. Takayanagi (Plenum, New York, 1984), Chap. 2.
[31] H. Ehrhardt, L. Langhans, F. Linder, and H. S. Taylor, Phys. Rev. **173**, 222 (1968).
[32] H. Tawara, Y. Itikawa, H. Nishimura, and M. Yoshino, J. Phys. Chem. Ref. Data **19**, 617 (1990).
[33] K. P. Huber and G. Herzberg, *Molecular Spectra and Molecular Structure, IV. Constants of Diatomic Molecules* (Van Nostrand Reinhold Company, New York, 1979).
[34] D. A. Douthat, J. Phys. B **12**, 663 (1979).
[35] I. Shimamura, Phys. Rev. A **23**, 3350 (1981); J. Phys. B **15**, 93 (1982).